npj | Clean Water

www.nature.com/npjcleanwater

ARTICLE OPEN

Sunlight-induced photoreduction of Cr(VI) to Cr(III) in wastewater by nitrogen-phosphorus-doped carbon dots

Anshu Bhati[1], Satyesh Raj Anand[1], Deepika Saini[1], Gunture[1] and Sumit Kumar Sonkar[1]

Cr(VI) is a known toxic and non-biodegradable pollutant that results from multiple industrial processes, and can cause significant environmental damage if it is not removed from wastewater. However, it can be reduced to Cr(III), which is less toxic and can be readily precipitated out and removed. Here, a fast and facile single-step technique is reported for the synthesis of nitrogen–phosphorus doped fluorescent carbon dots (NP-CD) using a domestic microwave, as a potential photocatalytic material. Under natural sunlight, a simple photocatalytic experiment reveals that the NP-CD are highly efficient for the quantitative reduction of Cr(VI) to Cr(III) in synthetic contaminated water, in a linear range from 10 ppm (in approximately 10 min) to 2000 ppm (in approximately 320 min) by increasing the sunlight irradiation time followed by its removal by precipitation. NP-CD exhibit high recyclability of up to six cycles without any apparent loss in photocatalytic activity, demonstrating NP-CD as a potential photocatalyst material for Cr(VI) water treatment.

npj Clean Water (2019)2:12 ; https://doi.org/10.1038/s41545-019-0036-z

INTRODUCTION

Since their discovery, photoluminescent carbon dots (CD)[1] are being researched all over because of their sustainable-advantageous applications and ease of fabrication.[2,3] CD are offering a vast viable platform for many potential applications, such as bioimaging, sensing, photocatalysis, LED, and photovoltaic.[2,3] The elemental compositions of CD modified with the long-known method of "doping" that involves the use of heteroatoms and metallic salts as dopants. Doping is a well-established method for articulating the optical and electrical properties of semiconductor nanoparticles.[2,4] Many reports are available stating that the doped-CD show remarkable results in terms of better quantum yield over the blue-green[5] and red[6,7] region of the visible spectrum along with its novel applications. Few groups have reported the doping of nitrogen (N) and phosphorus (P) to form nitrogen-phosphorous doped carbon dots (NP-CD), using hydrothermal,[8–10] solvothermal,[11] and microwave[12–15] assisted methods with the different precursor materials. NP-CD used for several applications such as for sensing Hg^{2+},[10] as a nano-carrier of anticancer drug[16], imaging purpose[8,12–14,16], oxygen reduction,[17] intercellular Fe^{3+} sensor,[8] fluorescence sensing of living cells,[13] and in the flourescence sensing of reactive oxygen and nitrogen species.[9] Presently, the doping of the CD are used to articulate its potential properties, with a huge expectation of the exploration of its newer prospects. For instance, in the field of water treatment[18,19] via aqueous phase photocatalysis,[6,7,20] which has been barely investigated. As per the general understanding, the heavy-metal-ion contamination in water is a severe threat, which indeed demands a viable, sustainable approach for its efficient sensing followed by its removal. For the same, sunlight-induced photocatalysis can be considered as a promising approach for the photodegradation of environmental pollutants.[21,22] The fabrication of novel nano-structured-materials with unique physical/chemical properties along with high efficiency towards the photocatalysis are the crucial step and required much attention.[6,7,18,23]

Beyond the conventional existing applications of CD, the present work investigate a newer perspective of NP-CD, using the natural sunlight for photoreduction of toxic Cr(VI) to Cr(III), followed by precipitation of Cr(III) salt. The toxic non-biodegradable[24] pollutant Cr(VI) is a well-known by-product of many industrial processes, like electroplating, paint making, leather tanning, and others, was discarded in the wastewater.[25] Cr(VI) is continuously damaging the aquatic system and shows devastating consequences.[26] Compared to the Cr(VI), Cr(III) is less toxic and can easily be precipitated out or adsorbed by the already existing methods.[27] So the conversion of Cr(VI) to Cr(III) followed by its simple precipitation is always in high demand. Nevertheless, it could be a sustainable approach, if the same can be performed under the presence of natural sunlight[6,7,18,23].

RESULTS AND DISCUSSION

A single-step process presented here describe the facile synthesis of the NP-CD from the pool of imidazole (source of nitrogen (N)), phosphoric acid (source of phosphorus (P)) and polyethylene glycol (source of carbon (C)), via the simplest method of microwave charring for ~4 min. The as-synthesized blue fluorescent NP-CD utilized for the aqueous phase photoreduction of Cr(VI) to Cr(III) under the presence of natural sunlight. Compared to artificial light, natural sunlight shows its significant contribution towards the photoreduction of the Cr(VI) to Cr(III) concerning the time required for the photoreduction is shown in Table 1, which also includes synthesis time for the fabrication of nano-carbons in comparison with the existing reports. Furthermore, the Cr(III) was also precipitated out by the NaOH solution to get treated water from the synthetic contaminated water.

Spectroscopic characterization

The absorption spectrum, (Fig. 1a) shows peaks at ~210 nm and ~270 nm that correspond to the transitions associated with π–π^*

[1]Department of Chemistry, Malaviya National Institute of Technology, Jaipur 302017, India
Correspondence: Sumit Kumar Sonkar (sksonkar.chy@mnit.ac.in)

Received: 16 October 2018 Accepted: 3 April 2019
Published online: 20 May 2019

Table 1. Comparative table showing synthesis and application of graphene based carbon nano material in the field of the photoreduction of Cr(VI)

'Source	Method	Synthesis condition	Catalyst	Loading catalyst	Cr(VI) conc.	Time	Source of light	Ref.
CNT, $TiOSO_4$, H_2SO_4, HCl/NH_4OH	Stirring	60 °C, 24 h	Coupling of TiO_2-CNT	1mg mL^{-1}	450 µM	60 min	Low flux (0.7mW cm^2) broad band 365 nm light	44
P25-TiO_2 and CQD	Hydrothermal	140 °C 4 h	CQD-TiO_2 nanocomposite	1.2 mg mL^{-1}	0.125 mM	40 min	Visible light 420 nm	45
Cetyltrimethyl ammonium bromide (CTAB), Si-CDs, NaOH, and TEOS	Stirring	80 °C 3 h	CDs-Silica hybrid	1 mg mL^{-1}	0.8 mM	180 min	Visible light Hg lamp, $\lambda > 400$	46
$FeCl_3.6H_2O$, ethanol, CH_3COONa, and Urea	Hydrothermal	180 °C 12 h	α-Fe_2O_3/g-C_3N_4	1mg mL^{-1}	10 ppm	150 min	visible light Xe lamp $\lambda \geq 400$ nm	47
GO, MWCNTs, and TBT	Hydrothermal	180 °C 8 h	Graphene-MWCNTs-TiO_2 hybrid	0.5 mg mL^{-1}	10 ppm	70 min	High pressure Hg lamp 230 W	48
C_3N_4, Ti-SBA 15, and DCDA	Furnace	550 °C 4 h	C_3N_4,Ti-SBA 15 composite	1 mg mL^{-1}	10 ppm	120 min	Xenon lamp 300 W	49
TiO_2 mesocrystals and CDs	Electrochemical, hydrothermal and evaporative	60 °C	CDs-TiO_2 meso-crystals	1 mg mL^{-1}	10 ppm	30 min	CEL-LED 365 nm	50
CNTs,TiO_2, $ZnSO_4$, and NaOH	Microwave assisted reaction	150 °C, 150 W, 10 min	ZnO-TiO_2-CNTs	1 mg mL^{-1}	10 ppm	250 min	High pressure 500 W Hg lamp	51
GO/ZnO/Ethanol	Ultrasonication followed by the photocatalytic reduction	30 min 7 h at 365 nm	ZnO-rGO nanocomposites	1 mg mL^{-1}	10 ppm	250 min	500 W high pressure Hg lamp, $\lambda = 365$ nm	52
UiO-66(NH_2) and GO	Hydrothermal	120 °C 24 h	MOF-rGO nanocomposites	0.5 mg mL^{-1}	10 ppm	100 min	Visible light $\lambda < 400$ nm	53
Bi_2WO_6 nanoparticle and rGO	Surface charge reaction followed with hydrothermal	160 °C 12 h	Bi_2WO_6-rGO composite	1 mg mL^{-1}	20 ppm	90 min	Xenon lamp 300 W	54
Melamine and sodium formate	Hydrothermal	150 °C 24 h	F-g-C_3N_4	1 mg mL^{-1}	20 ppm	240 min	Xenon lamp 300 W, $\lambda > 400$	55
MIL-53(Fe) and r-GO	Solvothermal	170 °C 24 h	MIL-53(Fe)-rGO	1 mg mL^{-1}	20 ppm	80 min	Xenon lamp 300 W	56
Melamine and 2-Aminoethylphophonic acid	Cube furnace	550 °C 8 h	Phosphorous doped porous g-C_3N_4 nanosheets	1 mg mL^{-1}	20 ppm	120 min	Xenon arc lamp, 300 W	57
Na_2SO_3/Se power/Na_2MoO_4/$NaBH_4$/HCl and CQD	Solvothermal	180 °C 12 h	CQD decorated $MoSe_2$	1 mg mL^{-1}	20 ppm	180 min	Visible light, UV and NIR light	58
MWCNTs-OH and Ti(O-Bu)$_4$	Hydrothermal	270 °C, 4 h	TiO_2CNTs	1 mg mL^{-1}	40 ppm	180 min	High pressure 125 W UV Bulb	59
WO_3, MWCNTs, $AgNO_3$, and Na_2HPO_4	Stirring in dark	25 °C 4 h	Ag_3PO_4–WO_3/MWCNTs	1 mg mL^{-1}	50 ppm	30 min	Visible light, 150 W halogen lamp, <420 nm	60
rGO, In_2O_3, and Cu_2O	Hydrothermal	180 °C 6 h	Cu_2O-rGO-In_2O_3 hybrid	25 mg mL^{-1}	50 ppm	360 min	Xenon lamp 300 W	61
Bougainvillea plant leaves/extract and 10% Zinc acetate	Microwave oven	1260 W 10 min	C_{ZnO}-Dots	3 mg mL^{-1}	100 ppm	300 min	Sunlight	6
GQDs/TNWs, Bi2S3 nanoparticle	Pulse electrode deposition	NA	Bi2S3/GQDs/TNWs ternary hybrids	NA	20 ppm	80 min	NA	62
CDs/EtOH/p-N-TiO2	Calcined	300 °C, 3 h	CDs-N-TiO2-x	50 mg	40 ppm	60 min	Visible light	63
Imidazole, poly ethylene glycol, phosphoric acid	Microwave oven	560 W 4 min	NP-CD	0.07 mg mL^{-1}	2000 ppm	320 min	Sunlight	This work

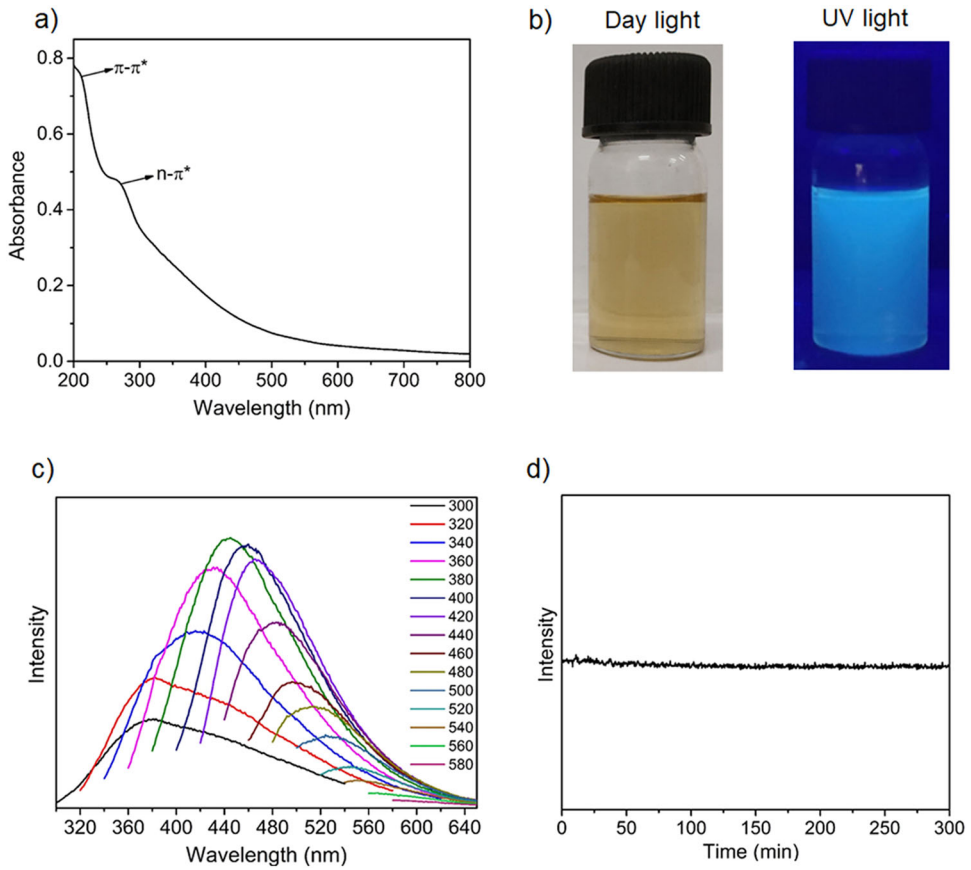

Fig. 1 **a** UV-Vis spectrum; **b** photographic image in daylight and UV light; **c** excitation dependent fluorescence emission spectra (excited from 300 nm to 580 nm with the increment of 20 nm towards the higher wavelength) and **d** photostability at 380 nm excitation for 5 hr of NP-CD

(C=C) and n–π* (C = N/P), respectively. The photographic images of the NP-CD in daylight and under the UV light illumination are shown in Fig. 1b. The blue emitting NP-CD show the excitation wavelength dependent flurorescence emission (Fig. 1c), situated mostly between the blue and green region (~360 to ~540 nm) of the visible spectrum, having the highest emission intensity at ~443 nm (excited at 380 nm), and possesing a quantum yield value of ~15%.[28] In addition, the photostability of NP-CD was investigated for 5 h at the excitation wavelength of 380 nm and it shows good photostability (Fig. 1d) without any apperent loss in the emission intensity.

The possible identification of the surface functionalities[29,30] of the NP-CD was carried out by X-ray photoelectron spectroscopy (XPS) and Fourier transform infrared spectroscopy (FTIR). XPS spectrum of NP-CD (Fig. 2a) shows the signature peaks associated with four elements; carbon (C_{1s}), oxygen (O_{1s}), nitrogen (N_{1s}), and phosphorus (P_{2p} and P_{2s}) at ~284.4 eV, ~532.1 eV, ~399.8 eV, ~132.6, and ~188 eV, respectively. The inset of Fig. 2a shows a tabular data for the elemental composition from the XPS survey scan. Figure 2b–e shows the high-resolution short scanned XPS spectra of C_{1s}, N_{1s}, P_{2p}, and O_{1s}, respectively after deconvulation. Short scanned C_{1s} analysis after deconvulation as displayed in Fig. 2b, showing the presence of six different peaks located at 283.4, 284.2, 284.8, 285.6, 286.2, and 288 eV corresponding to the presence of different binding states of carbon as C=C, C–C, C–N/P, C–O, C=N, and C=O, respectively.[31,32] After deconvulation short scan of N_{1s} show three major peaks at 398.9, 400.6 eV and 402 eV corresponding to the C=N–C (pyridinic N), C–N–H (pyrollic N), and C=N (graphitic N), respectively (Fig. 2c). Similarly, The P_{2p} short scan after deconvulation shows two peaks at 134.5 eV and 133.5 eV corresponding to the presence of the P–O and P–C, respectively (Fig. 2d).[9] The short scan for O_{1s} region after deconvulation shows the presence of three major peaks at 532.9 eV, 532.3 eV and 531.1 eV corresponding to the presence of C=O/C=N, C–O, and O–N/P, respectively (Fig. 2e).[33] FTIR results (Fig. 2f) show a broad band from 3484 to 3200 cm^{-1} corresponding to the N–H (sharp end) and O–H stretching vibrations.[12,16,34] The doublet at ~2925 and ~2873 cm^{-1} correspond to the C–H stretching vibrations.[34] The medium band at ~1745 cm^{-1} and ~1643 cm^{-1} correspond to C=O and C=C stretching vibrations. The medium band at ~1456 cm^{-1} and ~1351 cm^{-1} correspond to C=N and C–N stretching vibrations, respectively.[34–36] The medium and sharp peaks ~1068 cm^{-1} and ~940 cm^{-1} correspond to the C–O, P–O–C stretching vibrations. The bands between ~600 cm^{-1} and ~500 cm^{-1} correspond to the aromatic stretching,[12,16,17,35,37] along with presence of the signature peaks of –P–O–C– and =N–C– confirming the doping of N and P in the NP-CD. The presence of different type of functional groups confirmed by the FTIR spectra of NP-CD were also in accordance with binding suggested by the XPS spectra. Additionally, to understand the distribution of the different elements especially, the N and P within the carbonized matrix of NP-CD. We did a XPS analysis concerning the percentage composition of the different elements at three different places in the same sample and presented the data in the form of standard error as C (52.85 ± 0.36)%, O (30.23 ± 0.13)%, N (5.55 ± 0.06)%, P (11.36 ± 0.33)%.

Microscopic analysis

Transmission electron microscopy (TEM) was used to observe the morphology of NP-CD (Fig. 3). The TEM image of NP-CD (Fig. 3a), shows well dispersed spherical particles with the corresponding size distribution analysis in Fig. 3b. Gaussian fitting of the size

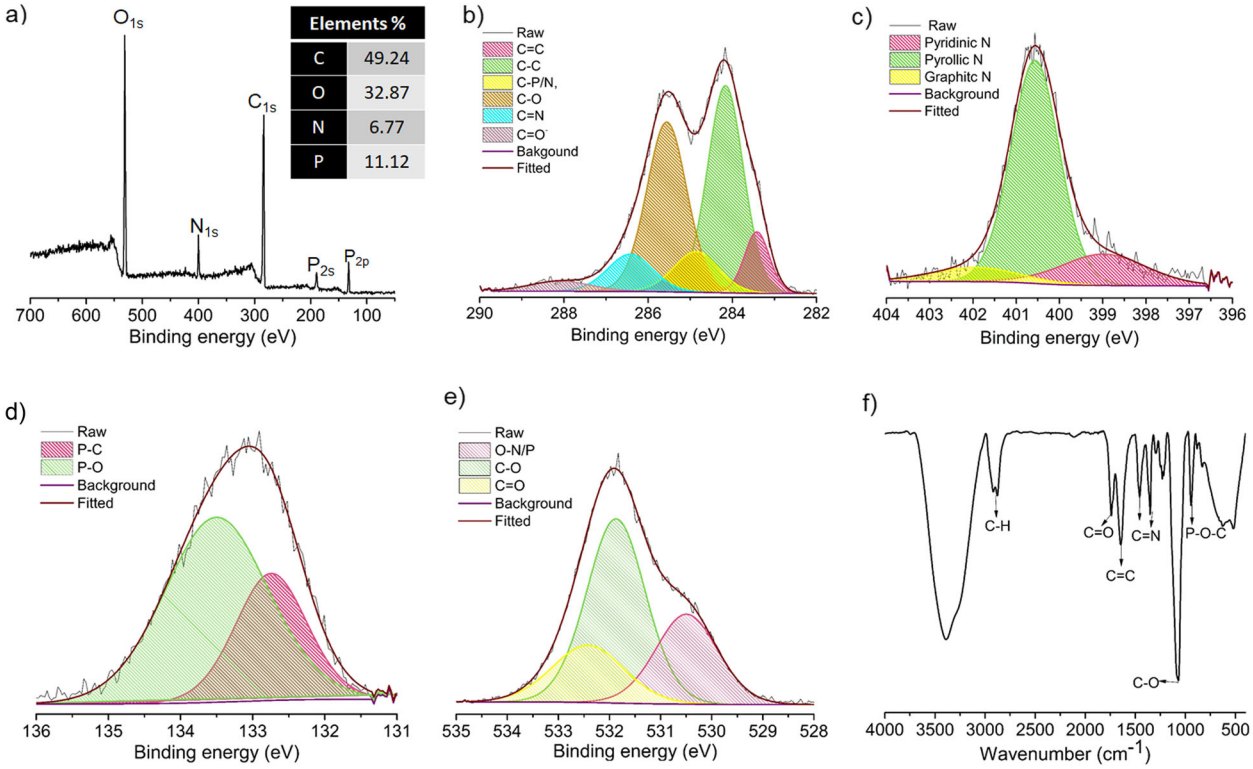

Fig. 2 **a** XPS survey scan of NP-CD with its corresponding short scan of **b** C1s; **c** N1s; **d** P2p and **e** O1s; **f** FTIR spectra

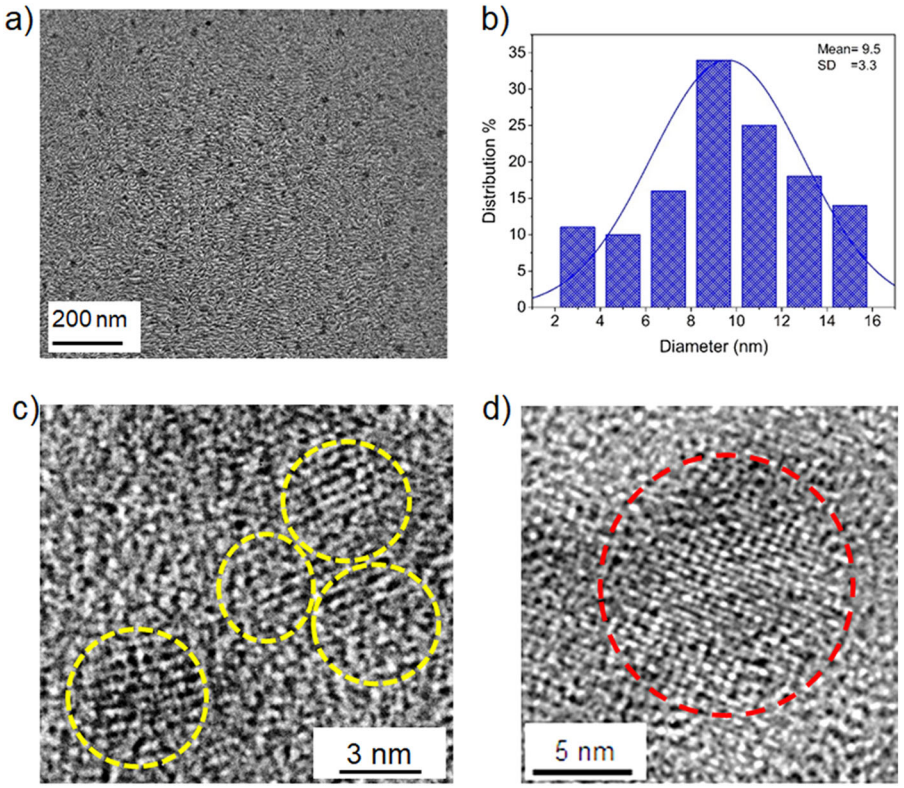

Fig. 3 **a** TEM image of NP-CD; and **b** its corresponding size distribution; **c** HRTEM image of NP-CD highlighted with yellow circles showing the arrangements of graphitic packing as interplanar fringes; **d** HRTEM image showing the interplanar arrangements of NP-CD

distribution curve shows that the average size of the NP-CD is 9.5 nm with the standard deviation of 3.3 nm. The High-resolution TEM (HRTEM) image in Fig. 3c shows the graphitic fringes encircled with the yellow circles. Figure 3d is the HRTEM image of NP-CD, which shows the interplanar layers of the graphitic carbon of 0.22 nm.

Sunlight Induced photocatalytic reduction of Cr(VI) and plausible mechanism

Using the potassium dichromate as a source of Cr(VI) to prepare the synthetic contaminated water, NP-CD were used here for the aqueous phase photocatalytic reduction of Cr(VI) to Cr(III) under the influence of natural sunlight. The important prospect of the present finding ascribed towards the photoreduction of variable concentrations of Cr(VI) (10 ppm–2000 ppm) to its respective Cr(III) using the same dose of the photocatalyst. The effects of NP-CD and sunlight on photocatalysis were shown in the Fig. 4a. The adsorption–desorption equilibrium was attained via sonicating for 30 min in the daylight (Fig. 4a, b) and afterwards the Cr(VI) was kept under the sunlight, and after every 10 min the photo reduced solutions were collected for the UV–Vis analysis. The residual Cr(VI) concentrations after the photoreduction were investigated by the UV–Vis spectrometer at 540 nm wavelength with the help of di-phenyl carbazide (DPC) assay.[6,38,39] In the absence of NP-CD (black line-Fig. 4a) and the sunlight (red line-Fig. 4a), there was almost negligible changes in the initial concentration of Cr(VI). While after the addition of the NP-CD in the presence of sunlight (blue line-Fig. 4a) almost complete photoreduction of the Cr (VI) (400 ppm) had been achieved within the ~110 min. Additionally, the same Fig. 4a shows that NP-CD exhibited only ~10% of adsorption. The quantitative evaluation of Cr(VI) reduction by NP-CD was performed using different concentrations (10, 50, 100, 400, 1000, 2000 ppm) of Cr (VI) with the same catalyst dose (0.07 mg mL^{-1}) just by increasing the sunlight irradiation time. The continuous decrease in the initial concentration of Cr(VI) represented as C/C_o with the time under the sunlight irradiation is shown in Fig. 4b. The photocatalytic reduction of Cr(VI) by NP-CD follows pseudo-first-order kinetics with a significant R^2 value (Fig. 4c). The rate constant and it's corresponding half-life for different Cr(VI) concentration were shown in Fig. 4d. The plausible mechanism for the photocatalytic Cr(VI) reduction by NP-CD, has been displayed in Fig. 4e. Under the influence of sunlight irradiation, holes and electrons are generated in the valence and conduction bands of NP-CD (equation (i)). Further, the photo induced holes react with water molecules to generate highly reactive H^+ (as shown in equation (ii)). The photo induced electrons were initially reacting with the Cr(VI) present near the periphery of the NP-CD as shown in equation (iii). These highly reactive protons and electrons cumulatively reduce Cr(VI) to Cr(III) as shown in equation (iv). The overall mechanism is showing schematically to understand the plausible reason for the photocatalytic reduction of toxic Cr(VI) to less toxic Cr(III). Nevertheless to state about the requirement of the acidic pH, as with the increase in pH towards basic side decreases the photoreduction efficiency of NP-CD[40]. The Cr(III) has been separated from the water by the precipitation in the form of the hydroxides of Cr(III) after the addition of NaOH solution.[41]

Effect of the contents of N, P on the photoreduction ability of NP-CD towards Cr(VI)

To investigate the effect of N and P content on the photoreduction ability of NP-CD, a control set of experiments was performed using single dopant material such as only N and only P charred with the same amount of polyethylene glycol (control sample) under the similar experimental conditions as being used for the synthesis of NP-CD. Figure 5a shows the prominent effect of combined doping of N-P compared to the un-doped (CD) and singly doped CD as (N-CD and P-CD). As well as, the effect of the amount of the reactant has also been investigated on the photoreduction efficiency by changing the reactant concentration to optimize the reaction conditions and obtain the maximum efficiency of photocatalyst. Figure 5b–d shows the effect of varying concentration of each reactant compared to the control (NP-CD). From the Fig. 5b–d it was concluded that the reactant mixture of 3 g imidazole, 10 mL phosphoric acid and 10 mL polyethylene glycol was the best composition for the fabrication of NP-CD for its potential application in photocatalytic reduction of Cr(VI) to Cr(III). Additionally, under the sunlight irradiation, Fig. 5e shows the extent of photocatalyst loading on the photoreduction efficiency of NP-CD and as expected it was found that on increasing the catalyst dose the rate of the photoreduction becomes faster compared to the lower dose for the same concentrations of Cr(VI) (400 ppm).[42] When the dose was 0.14 mg mL^{-1} the time required for 400 ppm Cr(VI) reduction was 20 min while at 0.07 mg mL^{-1} the time required for photocatalytic reduction was 110 min. For the presented finding a moderate amount of photocatalyst was being used (0.07 mg mL^{-1}). The NP-CD worked as a stable photocatalyst as observed by its recyclability upto six cycles which shows 98% efficiency for the 400 ppm Cr(VI), is demonstrated in Fig. 5f.

Effect of interfering ions

Further, to explore the possibilities of NP-CD in practical application, the photoreduction ability of NP-CD has been examined in the presence of many other interfering ions. Experimentally separate solutions of the 100 ppm of different interfering[43] ions (as chloride (Cl^-), sulfate (SO_4^{2-}), nitrate (NO_3^-), phosphate (PO_4^{3-}), ferrous (Fe^{2+}), and calcium (Ca^{2+})) along with a mixture that contains all the different interfering ions,[43] were mixed into the solutions of 400 ppm Cr(VI) under the similar experimental conditions as discussed above. All the experiments were carried out at the dose of photocatalyst (0.07 mg mL^1) in 120 min of sunlight irradiation. After performing the interference study, a minimal decrease in the reduction efficiency of NP-CD observed as shown in Fig. 6, with different interfering ions and their corresponding mixture compared with the control set containing 400 ppm Cr(VI) solution without any interfering ion. The NP-CD shows an effective and efficient photocatalytic material as the 100 ppm concentration of all the interfering ions and its corresponding mixtures does not affect the photoreduction abilities of NP-CD.

The present finding briefs about the synthesis and exploration of NP-CD as an efficient material for aqueous phase photocatalytic reduction of Cr(VI) to Cr(III) under the influence of natural sunlight. Moreover, the less toxic Cr(III) was removed from the treated water using a simpler process of precipitation. The ease in the recyclability along with no apparent loss in the catalytic efficiency could hold a large, prosperous future of these NP-CD in the field of photocatalytic water remediation. In future, the detailed structural characterization of NP-CD could further provide significant potential as priority materials to execute many hidden applications of doped-CD towards the efficient removal of various toxic inorganic and organic pollutants from the contaminated wastewater. Additionally, a detailed and systematic study to find out the wavelength dependence of the photodegradation efficiency could beimmensely helpful in providing valuable insights into the processes involved.

METHODS

Materials and reagents

All chemical reagents were of analytical grade, and used without further purification.

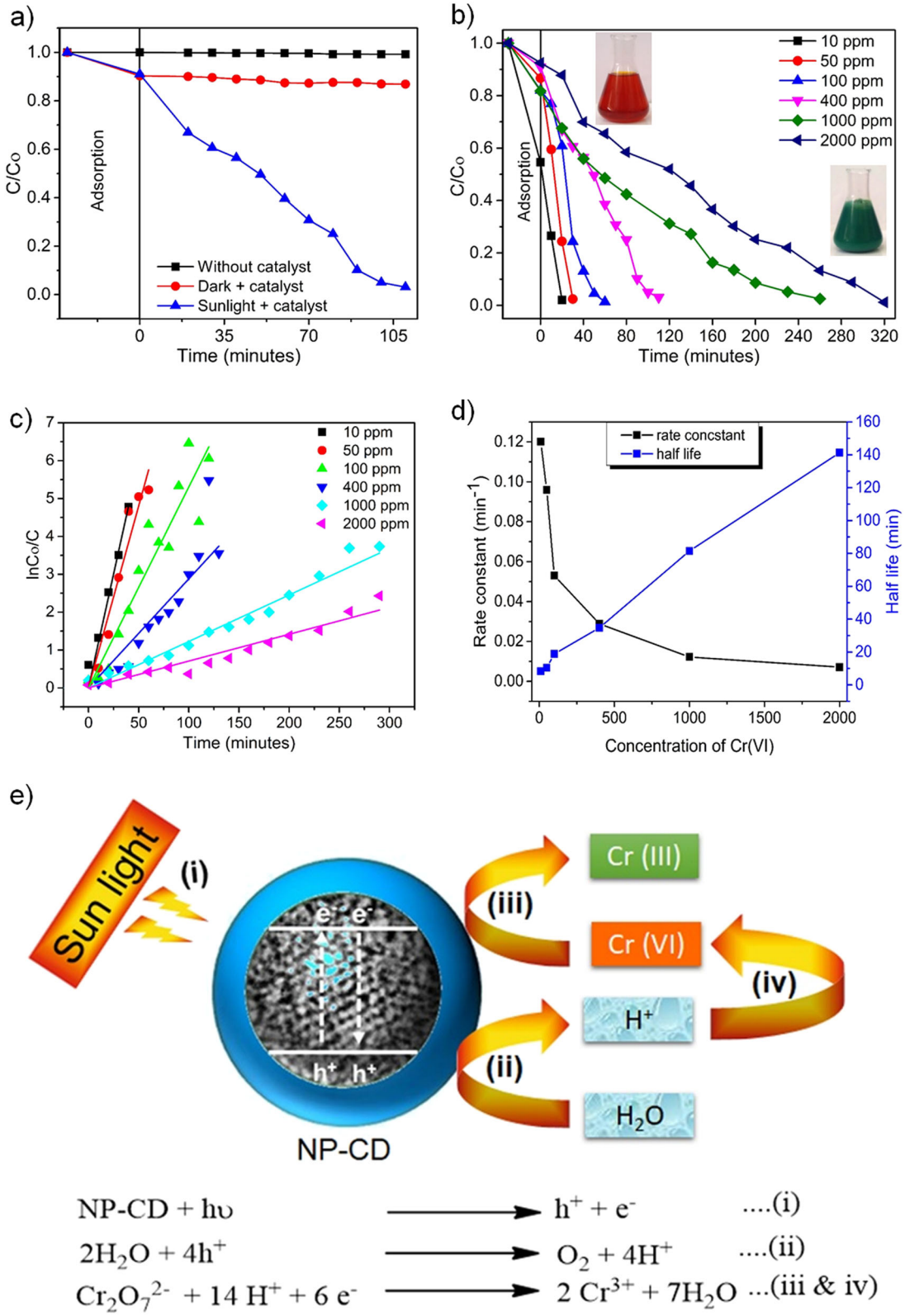

Fig. 4 **a** Plot of (C/Co) for the photoreduction of the 400 ppm of Cr(VI) by NP-CD under the different condition; **b** Plot of (C/Co) for Cr(VI) photoreduction by NP-CD under different concentrations of Cr(VI); **c** pseudo-first-order linear fit data with different concentration of Cr(VI); **d** rate constant and half-life graph for the different concentration of Cr (VI) and **e** schematic representation of plausible reaction mechanism of photocatalytic reduction of Cr(VI) to Cr(III) under the sunlight irradiation by NP-CD

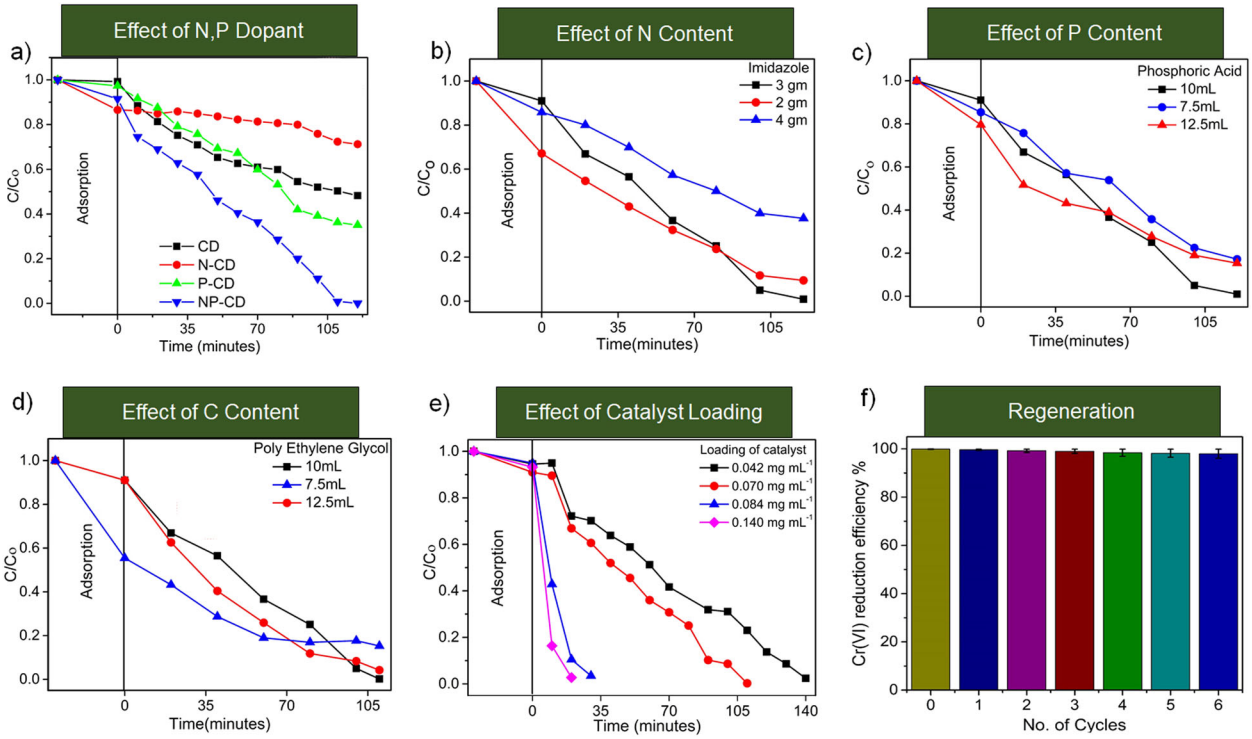

Fig. 5 **a** Effect of the reactant contents of N and P on the working efficiency of the CD; **b** effect of imidazole; **c** effect of phosphoric acid; **d** and the effect of polyethylene glycol; **e** effect of catalyst loading; **f** the photocatalytic performance up to six cycles by the recycling test on the photoreduction efficiency of NP-CD on the 400 ppm Cr(VI) under the sunlight irradiation

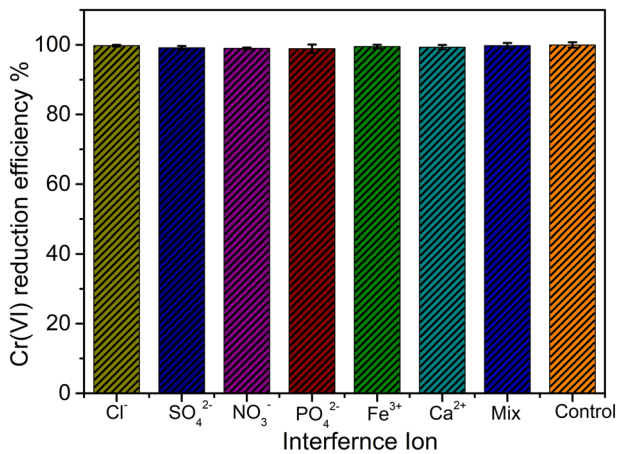

Fig. 6 Photoreduction efficiency of NP-CD under the different presence of the interfering ions Cl^-, SO_4^{2-}, NO_3^-, PO_4^{3-}, Fe^{2+} and Ca^{2+} along with its mixture which contains 100 ppm of each the interfering ionunder the presence of sunlight

Instrumentation

Perkin Elmer Lambda 35 spectrometer used for the UV–Vis absorption spectra. Fluoromax 4 C.L.System were used for the photoluminescence spectrometry analyses in aqueous solutions, ESCA$^+$ omicron nanotechnology oxford instrument were used for the XPS measurements. Bruker Vertex 70 FT-IR spectrophotometer were used for the recording of FTIR spectra using KBr pellets. The morphology of the NP-CD were studied by the Tecnai 20 G2 300 kV, STWIN model transmission electron microscope. HRTEM analyses were done at 300 kV acceleration voltage.

Synthesis of NP-CD

The NP-CD were synthesized from the pool of the mixed reagents containing 3 g of imidazole, 10 mL phosphoric acid and 10 mL polyethylene glycol (molecular weight ~400 g/mol) in a 100 mL beaker. A domestic microwave oven at 560 W power was used to carbonize the mixture after 10 min sonication. The transparent solution containing (imidazole, phosphoric and polyethylene glycol), now turned into the dark brown solution. The supernatant was then centrifuged at 6000 rpm for 15 min to obtain a clear solution collected and dried on the water bath to obtain NP-CD. Further, the as-synthesized NP-CD get neutralized with the ammonia solution to remove the excess phosphoric acid followed by repetitively washing with DI water for the preparation of the pallets for XPS analysis. The synthetic procedure for the formation of different CD was the same only the difference in the starting materials, Such as in CD (only PEG was used), in the case of N-CD (imidazole + PEG) and for P-CD (phosphoric acid + PEG) was used under the similar conditions used for the fabrication of NP-CD. The QY of the NP-CD were calculated by the given formula.

$$Q = Q_r * \frac{I}{I_r} * \frac{A_r}{A} * \frac{\cap^2}{\cap_r^2},$$

where Q is the QY, I is the measured integrated emission intensity, $\cap$ is the refractive index of the solvent and A is the optical density. The subscript "r" refers to the reference standard with known QY. Herein the quinine sulfate was dissolved in 0.1 M H_2SO_4 as the reference standard with a known QY of 0.54.

Photocatalytic activity measurement

The photocatalytic activity of NP-CD were investigated by the reduction of the synthetic contaminated water from its orange colored Cr(VI) to green colored Cr(III) in aqueous solution under direct irradiation of sunlight. A stock solution of 2000 ppm Cr(VI) was prepared dissolving 1.42 g potassium dichromate in the 250 mL of DI water. The lower concentration of the Cr(VI) was prepared by diluting the stock solution. In a typical process, 3.5 mg of the NP-CD were mixed in the 50 mL of different Cr(VI) solutions and sonicated for 30 min to obtain the adsorption–desorption equilibrium, afterwards the solution were kept into the sunlight irradiation for the photoreduction. To study the kinetic rate of the photocatalytic reduction, we collected the 2 mL of the samples at the time interval of 10 minutes. The obtained samples were centrifuged and further diluted. The diluted solution was treated with DPC assay[6,38,39] to detect the Cr(VI) concentration at 540 nm in the UV–Vis spectrophotometer.

DATA AVAILABILITY

The authors declare that all the data supporting the findings of this study are available within the article. Extra data are available from the corresponding author upon request.

ACKNOWLEDGEMENTS

A.B. thanks MNIT Jaipur for a doctoral fellowship. S.R.A. thanks DST, New Delhi for funding, D.S. thanks DST-Inspire for doctoral fellowship. G. thanks CSIR for doctoral fellowship. S.K.S. thanks DST (SB/EMEQ-383/2014) for funding. S.K.S. thanks Material Research Center (MRC), MNIT Jaipur, for material characterization.

AUTHOR CONTRIBUTIONS

S.K.S. proposed and supervised all the experiment of the work; A.B., S.R., and D.S. performed most of the experiment work; G. assisted the whole experiment and contributed to the sample analyses. All authors reviewed the manuscript.

ADDITIONAL INFORMATION

Competing interests: The authors declare no competing interests.

Publisher's note: Springer Nature remains neutral with regard to jurisdictional claims in published maps and institutional affiliations.

REFERENCES

1. Sun, Y.-P. et al. Quantum-sized carbon dots for bright and colorful photoluminescence. *J. Am. Chem. Soc.* **128**, 7756–7757 (2007).
2. Park, Y., Yoo, J., Lim, B., Kwon, W. & Rhee, S. W. Improving the functionality of carbon nanodots: doping and surface functionalization. *J. Mater. Chem. A* **4**, 11582–11603 (2016).
3. Wang, R., Lu, K.-Q., Tang, Z.-R. & Xu, Y.-J. Recent progress in carbon quantum dots: synthesis, properties and applications in photocatalysis. *J. Mater. Chem. A* **5**, 3717–3734 (2017).
4. Zhijie, Z., Tingting, Z., Xiaoming, L., Jiayue, X. & Haibo, Z. Progress of carbon Quantum dots in photocatalysis applications. *Part. Part. Syst. Char.* **33**, 457–472 (2016).
5. Wang, Y., Zhu, Y., Yu, S. & Jiang, C. Fluorescent carbon dots: rational synthesis, tunable optical properties and analytical applications. *RSC Adv.* **7**, 40973–40989 (2017).
6. Khare, P., Bhati, A., Anand, S. R., Gunture & Sonkar, S. K. Brightly fluorescent zinc-doped red-emitting carbon dots for the sunlight-induced photoreduction of Cr (VI) to Cr(III). *ACS Omega* **3**, 5187–5194 (2018).
7. Bhati, A. et al. Sunlight-induced photocatalytic degradation of pollutant dye by highly fluorescent red-emitting Mg-N-embedded carbon dots. *ACS Sustain. Chem. Eng*. **6**, 9246–9256 (2018).
8. Chandra, S. et al. Synthesis of highly fluorescent nitrogen and phosphorus doped carbon dots for the detection of Fe3+ ions in cancer cells. *Luminescence* **31**, 81–87 (2016).
9. Gong, Y., Yu, B., Yang, W. & Zhang, X. Phosphorus, and nitrogen co-doped carbon dots as a fluorescent probe for real-time measurement of reactive oxygen and nitrogen species inside macrophages. *Biosens. Bioelectron.* **79**, 822–828 (2016).
10. Xu, Q. et al. Synthesis, mechanical investigation, and application of nitrogen and phosphorus co-doped carbon dots with a high photoluminescent quantum yield. *Nano Res.* **1**, 3691–3701 (2017).
11. Wu, H. et al. Solvothermal synthesis of green-fluorescent carbon nanoparticles and their application. *J. Lumin.* **132**, 1603–1607 (2012).
12. Li, H. et al. Microwave-assisted synthesis of N,P-doped carbon dots for fluorescent cell imaging. *Microchim. Acta* **183**, 821–826 (2016).
13. Liu, R. et al. Nitrogen and phosphorus co-doped graphene quantum dots as a nano-sensor for highly sensitive and selective imaging detection of nitrite in live cell. *Sens. Actuators B* **240**, 604–612 (2017).
14. Ananthanarayanan, A. et al. Nitrogen and phosphorus co-doped graphene quantum dots: synthesis from adenosine triphosphate, optical properties, and cellular imaging. *Nanoscale* **7**, 8159–8165 (2015).
15. Sun, X., Brückner, C. & Lei, Y. One-pot and ultrafast synthesis of nitrogen and phosphorus co-doped carbon dots possessing bright dual wavelength fluorescence emission. *Nanoscale* **7**, 17278–17282 (2015).
16. Gong, X. et al. Phosphorus and nitrogen dual-doped hollow carbon dot as a nanocarrier for doxorubicin delivery and biological imaging. *ACS Appl Mater. Interfaces* **8**, 11288–11297 (2016).
17. Li, R., Wei, Z. & Gou, X. Nitrogen and phosphorus dual-doped graphene/carbon nanosheets as bifunctional electrocatalysts for oxygen reduction and evolution. *ACS Catal.* **5**, 4133–4142 (2015).
18. Khare, P. et al. Sunlight-induced selective photocatalytic degradation of methylene blue in bacterial culture by pollutant soot derived nontoxic graphene nanosheets. *ACS Sustain. Chem. Eng.* **6**, 579–589 (2018).
19. Tripathi, K. M., Gupta, N. R. & Sonkar, S. K. *Smart Materials for Waste Water Applications*, Vol. 1 Ch. 5, 127–154 (Wiley, Hoboken, 2016).
20. Han, M. et al. Recent progress on the photocatalysis of carbon dots: classification, mechanism and applications. *Nano Today* **19**, 201–218 (2018).
21. Liu, S. et al. Enhanced photocatalytic degradation of environmental pollutants under visible irradiation by a composite coating. *Environ. Sci. Technol.* **51**, 5137–5145 (2017).
22. Ameta, R., Benjamin, S., Ameta, A. & Ameta, S. Photocatalytic Degradation of Organic Pollutants: A Review. *Material science Forum*. **734**, 247–272 (2012).
23. Tripathi, K. M., Singh, A., Bhati, A., Sarkar, S. & Sonkar, S. K. Sustainable feasibility of the environmental pollutant soot to few-layer photoluminescent graphene nanosheets for multifunctional applications. *ACS Sustain. Chem. Eng.* **4**, 6399–6408 (2016).
24. Omole, M. A., K'Owino, I. O. & Sadik, O. A. Palladium nanoparticles for catalytic reduction of Cr(VI) using formic acid. *Appl. Catal. B* **76**, 158–167 (2007).
25. Yang, Y., Wang, G., Deng, Q., Ng, D. H. L. & Zhao, H. Microwave-assisted fabrication of nanoparticulate TiO_2 microspheres for synergistic photocatalytic removal of Cr(VI) and methyl orange. *ACS Appl Mater. Interfaces* **6**, 3008–3015 (2014).
26. Abdullah, H. & Kuo, D.-H. Facile synthesis of n-type (AgIn)xZn2(1–x)S2/p-type Ag2S nanocomposite for visible light photocatalytic reduction to detoxify hexavalent chromium. *ACS Appl Mater. Interfaces* **7**, 26941–26951 (2015).
27. Ma, H.-L. et al. Chemical reduction and removal of Cr(vi) from acidic aqueous solution by ethylenediamine-reduced graphene oxide. *J. Mater. Chem.* **22**, 5914–5916 (2012).
28. Crosby, G. A. & Demas, J. N. Measurement of photoluminescence quantum yields. *Rev. J. Phys. Chem.* **75**, 991–1024 (1971).
29. Nxumalo, E. & Coville, N. Nitrogen doped carbon nanotubes from organometallic compounds: a review. *Materials* **3**, 2141–2171 (2010).
30. Zikalala, S. A., Kuvarega, A. T., Mamba, B. B., Mhlanga, S. D. & Nxumalo, E. N. The effect of synthetic routes on the physicochemical properties and optical response of N-doped titania-oxidized carbon nanotube nanohybrids. *Mater. Today Chem.* **10**, 1–18 (2018).
31. Tripathi, K. M. et al. From the traditional way of pyrolysis to tunable photoluminescent water soluble carbon nano-onions for cells imaging and selective sensing of glucose. *RSC Adv.* **6**, 37319–37340 (2016).
32. Tripathi, K. M. et al. Sustainable changes in the contents of metallic micronutrients in first generation gram seeds imposed by carbon nano-onions: a life cycle seed to seed study. *ACS Sustain. Chem. Eng.* **5**, 2906–2916 (2017).
33. Zheng, B. et al. One pot selective synthesis of water and organic soluble carbon dots with green fluorescence emission. *RSC Adv.* **5**, 11667–11675 (2015).
34. Song, Z. et al. Multifunctional N,S co-doped carbon quantum dots with pH- and thermo-dependent switchable fluorescent properties and highly selective detection of glutathione. *Carbon* **104**, 169–178 (2016).
35. Sun, D. et al. Hair fiber as a precursor for synthesizing of sulfur- and nitrogen-co-doped carbon dots with tunable luminescence properties. *Carbon* **64**, 424–434 (2013).
36. Dong, Y. et al. Carbon-based dots co-doped with nitrogen and sulfur for high Quantum yield and excitation-independent emission. *Angew. Chem. Int. Ed.* **52**, 7800–7804 (2013).
37. Lin, Z., Waller, G., Liu, Y., Liu, M. & Wong, C.-P. Facile synthesis of nitrogen-doped graphene via pyrolysis of graphene oxide and urea, and its electrocatalytic activity toward the oxygen-reduction reaction. *Adv. Energy Mater.* **2**, 884–888 (2012).
38. Verma, N. K., Khare, P. & Verma., N. Synthesis of iron-doped resorcinol formaldehyde-based aerogels for the removal of Cr(VI) from wate. *Green. Process Synth.* **4**, 37–46 (2015).
39. Khare, P., Yadav, A., Ramkumar, J. & Verma, N. Microchannel-embedded metal–carbon–polymer nanocomposite as a novel support for chitosan for efficient removal of hexavalent chromium from water under dynamic conditions. *Chem. Eng. J.* **293**, 44–54 (2016).
40. Shao, D., Wang, X. & Fan, Q. Photocatalytic reduction of Cr(VI) to Cr(III) in solution containing ZnO or ZSM-5 zeolite using oxalate as model organic compound in environment. *Microporous Mesoporous Mater.* **117**, 243–248 (2009).
41. Zhong, Y. et al. Flexible electrospun carbon nanofiber/Tin(IV) sulfide core/sheath membranes for photocatalytically treating chromium(VI)-containing wastewater. *ACS Appl Mater. Interfaces* **8**, 28671–28677 (2016).

42. Shirzad-Siboni, M., Farrokhi, M., Darvishi Cheshmeh Soltani, R., Khataee, A. & Tajassosi, S. Photocatalytic reduction of hexavalent chromium over ZnO nanorods immobilized on kaolin. *Ind. Eng. Chem. Res.* **53**, 1079–1087 (2014).
43. Djellabi, R. & Ghorab, M. F. Photoreduction of toxic chromium using TiO2-immobilized under natural sunlight: effects of some hole scavengers and process parameters. *Desalin. Water Treat.* **55**, 1900–1907 (2015).
44. Shaham-Waldmann, N. & Paz, Y. Beyond charge separation: the effect of coupling between titanium dioxide and CNTs on the adsorption and photocatalytic reduction of Cr(VI). *Chem. Eng. J.* **231**, 49–58 (2013).
45. Choi, D., Ham, S. & Jang, D.-J. Visible-light photocatalytic reduction of Cr(VI) via carbon quantum dots-decorated TiO2 nanocomposites. *J. Enviorn Chem. Eng.* **6**, 1–8 (2018).
46. Liu, Y. et al. The effective removal of Cr(vi) ions by carbon dot–silica hybrids driven by visible light. *RSC Adv.* **6**, 68530–68537 (2016).
47. Xiao, D., Dai, K., Qu, Y., Yin, Y. & Chen, H. Hydrothermal synthesis of α-Fe2O3/g-C3N4 composite and its efficient photocatalytic reduction of Cr(VI) under visible light. *Appl. Surf. Sci.* **358**, 181–187 (2015).
48. Wang, C. et al. Preparation of graphene–carbon nanotube–TiO2 composites with enhanced photocatalytic activity for the removal of dye and Cr (VI). *Appl. Catal. A* **473**, 83–89 (2014).
49. Liu, F. et al. Carbon nitride coupled Ti-SBA15 catalyst for visible-light-driven photocatalytic reduction of Cr (VI) and the synergistic oxidation of phenol. *Appl. Catal. B* **201**, 1–11 (2017).
50. Zhang, Y., Xu, M., Li, H., Ge, H. & Bian, Z. The enhanced photoreduction of Cr(VI) to Cr(III) using carbon dots coupled TiO2 mesocrystals. *Appl. Catal. B* **226**, 213–219 (2018).
51. Liu, X., Pan, L., Lv, T., Sun, Z. & Sun, C. Enhanced photocatalytic reduction of Cr(VI) by ZnO–TiO2–CNTs composites synthesized via microwave-assisted reaction. *J. Mol. Catal. A* **363-364**, 417–422 (2012).
52. Liu, X. et al. UV-assisted photocatalytic synthesis of ZnO-reduced graphene oxide composites with enhanced photocatalytic activity in reduction of Cr(VI). *Chem. Eng. J.* **183**, 238–243 (2012).
53. Shen, L. et al. Electrostatically derived self-assembly of NH2-mediated zirconium MOFs with graphene for photocatalytic reduction of Cr(vi). *RSC Adv.* **4**, 2546–2549 (2014).
54. Yang, J., Wang, X., Zhao, X., Dai, J. & Mo, S. Synthesis of uniform Bi2WO6-reduced graphene oxide nanocomposites with significantly enhanced photocatalytic reduction activity. *J. Phys. Chem. C* **119**, 3068–3078 (2015).
55. Dong, G. & Zhang, L. Synthesis and enhanced Cr(VI) photoreduction property of formate anion containing graphitic carbon nitride. *J. Phys. Chem. C* **117**, 4062–4068 (2013).
56. Liang, R., Shen, L., Jing, F., Qin, N. & Wu, L. Preparation of MIL-53(Fe)-reduced graphene oxide nanocomposites by a simple self-assembly strategy for increasing interfacial contact: efficient visible-light photocatalysts. *ACS Appl. Mater. Interfaces* **7**, 9507–9515 (2015).
57. Deng, Y. et al. Insight into highly efficient simultaneous photocatalytic removal of Cr(VI) and 2,4-diclorophenol under visible light irradiation by phosphorus doped porous ultrathin g-C3N4 nanosheets from aqueous media: Performance and reaction mechanism. *Appl. Catal. B* **203**, 343–354 (2017).
58. Ren, Z. et al. Carbon quantum dots decorated MoSe2 photocatalyst for Cr(VI) reduction in the UV–vis-NIR photon energy range. *J. Colloid Interface Sci.* **488**, 190–195 (2017).
59. Huang, L., Chan, Q., Wu, X., Wang, H. & Liu, Y. The simultaneous photocatalytic degradation of phenol and reduction of Cr(VI) by TiO2/CNTs. *J. Ind. Eng. Chem.* **18**, 574–580 (2012).
60. Cai, L., Xiong, X., Liang, N. & Long, Q. Highly effective and stable Ag_3PO_4–WO3/MWCNTs photocatalysts for simultaneous Cr(VI) reduction and orange II degradation under visible light irradiation. *Appl. Surf. Sci.* **353**, 939–948 (2015).
61. Liu, J. et al. Oxygen vacancies in shape controlled Cu_2O/reduced graphene oxide/In_2O_3 hybrid for promoted photocatalytic water oxidation and degradation of environmental pollutants. *ACS Appl Mater. Interfaces* **9**, 11678–11688 (2017).
62. Geng, H. et al. Architecting Bi2S3/graphene quantum dots/TiO2 photoelectrodes for aqueous Cr(VI)/methyl orange removal. *Mater. Lett.* **214**, 146–149 (2018).
63. Xu, L. et al. Facial fabrication of carbon quantum dots (CDs)-modified N-TiO2-x nanocomposite for the efficient photoreduction of Cr(VI) under visible light. *Chem. Eng. J.* **357**, 473–486 (2019).

Open Access This article is licensed under a Creative Commons Attribution 4.0 International License, which permits use, sharing, adaptation, distribution and reproduction in any medium or format, as long as you give appropriate credit to the original author(s) and the source, provide a link to the Creative Commons license, and indicate if changes were made. The images or other third party material in this article are included in the article's Creative Commons license, unless indicated otherwise in a credit line to the material. If material is not included in the article's Creative Commons license and your intended use is not permitted by statutory regulation or exceeds the permitted use, you will need to obtain permission directly from the copyright holder. To view a copy of this license, visit http://creativecommons.org/licenses/by/4.0/.

© The Author(s) 2019